Morphology and thermal conductivity of model organic aerogels

Anthony P. Roberts
Faculty of Environmental Sciences, Griffith University, Nathan, Queensland 4111, Australia
(Received 18 September 1996)

The intersection volume of two independent two-level cut Gaussian random fields is proposed to model the open-cell microstructure of organic aerogels. The experimentally measured x-ray scattering intensity, surface area, and solid thermal conductivity of both *polymeric* and *colloidal* organic aerogels can be accounted for by the model. [S1063-651X(97)50702-1]

PACS number(s): 82.70.Gg, 44.30.+v, 61.10.Eq, 61.43.Bn

Aerogels are a promising material for a host of applications [1,2] due to their thermal, optical, and mechanical properties. For example, aerogels are among the best thermal insulating solid materials known [3–5]. It is important to link aerogel properties to their complex internal microstructure, and to understand how such properties can be optimized for a given application [2,4,6]. The nanoscale porous morphology of aerogels has been extensively characterized by x-ray scattering and surface area analysis [7–10]. Despite this, aerogel properties are usually correlated with density, rather than related to morphological features. One reason for this is the lack of a suitable representation of aerogel morphology. In this paper we develop a model which accounts for the open-cell morphology of organic aerogels. The solid thermal conductivity of the model is computed and shown to be in good agreement with experimental data.

Thermal transport in aerogels is due to three additive components: conduction in the solid skeleton and (gas-filled) pores and conduction due to radiation [3]. For thermal insulation purposes it is desirable to reduce the magnitude of each contribution. Gaseous conductivity can be significantly reduced by decreasing pore size or partially evacuating the material, and radiative transport reduced by the inclusion of an opacifier [3,4]. The solid conductivity (typically half the total) depends strongly on the aerogel density and microstructure [4,6].

Organic aerogels produced by the polymerization of resorcinal and formaldehyde (RF) have been suggested as an alternative insulator to opacified silica aerogels [3,11]. They have lower intrinsic and radiative conductivities, and are less brittle than their silica based counterparts [3,4]. Both the morphology [8,12] and properties of organic aerogels [3,6,13–15] have been the subject of detailed investigation. A key variable in the formation of RF aerogel microstructure is the initial ratio of resorcinal to catalyst (R/C) [8]. As the catalyst increases the aerogels vary from a colloidal structure to a well-connected polymeric structure with a corresponding increase in conductivity and strength [6,13]. It is important to quantitatively model these properties to assist in the understanding and optimization of RF aerogels.

Current models of aerogels are based on simulating the microstructure formation using the diffusion-limited cluster-cluster aggregation (DLCA) scheme [10,16–18]. Two features of DLCA models (proposed for silica aerogels) suggest that they are not well suited to modeling RF aerogels. First, the DLCA model exhibits fractal scaling [16,17] and a well pronounced peak in the scattering intensity [10,18]. In contrast, RF aerogels exhibit no fractal scaling, and under high catalyst conditions the peak is weak, or even absent [8]. Second, the discrete character of DCLA-type models (open networks of cubes or hard spheres) may be ill-suited to modeling ''continuum'' properties within the aerogel skeleton. For example, the influential interparticle neck size [14] is equal to zero for hard spheres [10], and equal to the particle size for cubes [16–18]. We propose a statistical model of microstructure which can account for the main morphological features of RF aerogels. The model is lattice independent, and suitable for continuum-based theoretical and computational prediction of properties [19,20].

A convenient statistical description of porous media is provided by modeling the internal interface as the isosurface (or level-cut) of a Gaussian random field (GRF) $y(\boldsymbol{r})$. This model has been used to describe the morphologies arising in spinodal decomposition [21], microemulsions [22,23], galaxy formation [24], and porous rocks [25], among others [26]. The statistics of the material are completely determined by the specification of the single level-cut parameter and the field-field correlation function $g(r)=\langle y(\boldsymbol{0})y(\boldsymbol{r})\rangle$ [where $r=|\boldsymbol{r}|$ and $g(0)\equiv 1$]. Berk generalized the model to account for the x-ray scattering properties of microemulsions [27] by defining phase 1 to occupy the region in space where $\alpha \leqslant y(\boldsymbol{r}) \leqslant \beta$ and phase 2 to occupy the remainder. This model has also been shown to account for the morphology and properties of foamed solids [28] and polymer blends [29].

Neither the 1-cut GRF model, or Berk's ''2-cut'' extension, can account for the high porosity open-cell microstructure of aerogels. The 1-cut GRF is not macroscopically connected at aerogel porosities [20] (typically 95%), and Berk's 2-cut model exhibits sheetlike structures [30] similar to those observed in closed-cell foams [31]. To model the open-cell microstructure we define the solid phase to occupy the region $\alpha \leqslant y(\boldsymbol{r}) \leqslant \beta$ *and* $\alpha \leqslant w(\boldsymbol{r}) \leqslant \beta$, where y and w are statistically independent GRF's. The independence of the random fields allows the correlation functions of the model to be calculated. The solid volume fraction of the model is just $p=(p_\beta - p_\alpha)^2$, where $p_\alpha=(2\pi)^{-1/2}\int_{-\infty}^{\alpha} e^{-t^2/2}dt$ and the two-point correlation function is $p_2(r)=h_2^2(r)$, where $h_2(r)$ is the two-point function of Berk derived for the same values of α and β,

$$h_2(r)=h^2+\frac{1}{2\pi}\int_0^{g(r)}\frac{dt}{\sqrt{1-t^2}}\times\left[\exp\left(-\frac{\alpha^2}{1+t}\right)-2\exp\left(-\frac{\alpha^2-2\alpha\beta t+\beta^2}{2(1-t^2)}\right)+\exp\left(-\frac{\beta^2}{1+t}\right)\right] \quad (1)$$

with $h=p_\beta-p_\alpha$. The freedom in specifying the level-cut parameters and the field-field correlation function of the model $g(r)$ allow a wide variety of morphologies to be modeled.

To relate the model to experimental data it is necessary to specify a field-field correlation function. Prior studies [22,32] suggest a form

$$g(r)=\frac{e^{-r/\xi}-(r_c/\xi)e^{-r/r_c}}{1-(r_c/\xi)}\frac{\sin 2\pi r/d}{2\pi r/d} \quad (2)$$

characterized by a correlation length ξ, domain scale d, and a cutoff scale r_c. Two commonly measured morphological quantities of porous media are the surface area S and the x-ray scattering intensity $I(q)$. These can be computed for the model as

$$\frac{S}{V}=\frac{4\sqrt{2p}}{\pi}(e^{-(1/2)\alpha^2}+e^{-(1/2)\beta^2})\sqrt{\frac{4\pi^2}{6d^2}+\frac{1}{2r_c\xi}} \quad (3)$$

and

$$\frac{I(q)}{V}=\langle\eta^2\rangle\int_0^\infty 4\pi r^2[p_2(r)-p^2]\frac{\sin qr}{qr}dr, \quad (4)$$

where V is the sample volume and η is the scattering density of the solid phase [33].

To model RF aerogels we choose the model parameters to match experimentally measured scattering and surface area data [8]. While the domain scale d corresponds to the pore scale in aerogels, the geometry of the fibers depends on both the length scale and level-cut parameters. Uncertainties in the estimation of surface area [9,12,34] and skeletal density of aerogels suggest that only rough approximations of the parameters are justified. Examples of a colloidal and polymeric aerogel are chosen to ascertain the generality of the model. The colloidal aerogel is produced under low catalyst conditions ($R/C=300$) and has density $\rho_a=148$ kg m^{-3} ($p=\rho_a/\rho_s=0.11$) [8]. TEM images show a ''string-of-pearls'' appearance: a network comprised of grains (diameter 120–300 Å) interconnected by narrow necks. The surface area is 400 m^2/g and x-ray scattering yields a peak at $q=0.012$ Å^{-1} (Fig. 1) [8]. A good match between the experimental information and the model was obtained for $r_c=10, \xi=14$, $d=46$ nm, and $p_{\alpha,\beta}=0.07,0.40$. The model surface area is 428 m^2/g, and the theoretical scattering curve is seen to be in good agreement with the experimental data (Fig. 1). In Fig. 2 we show a slab of the material: the model reproduces the colloidal string-of-pearls morphology with reasonable grain and neck sizes. We directly measure the scattering from the model. The results are included in Fig. 1, demonstrating that the simulation reproduces the theoretical statistics very well. At small q (large length scales) some deviation is evident; this is due to the finite size of the samples [35].

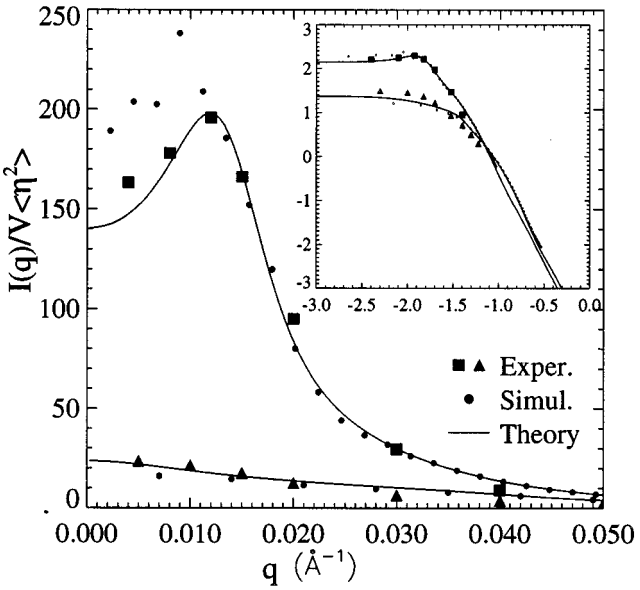

FIG. 1. X-ray scattering spectra of RF aerogels. The data for the upper and lower curves are for a colloidal ($R/C=300$, $p=11\%$) and polymeric ($R/C=50$, $p=7.7\%$) aerogel, respectively [8] (the experimental data are vertically scaled). The theoretical curves were obtained using Eq. (4), and the simulation data are measured directly from one realization of each model (Figs. 2 and 3). The inset shows $\log_{10}(I(q)/V\langle\eta^2\rangle)$ vs $\log_{10}(q)$.

The polymeric aerogel [8] we model is produced under high catalyst conditions ($R/C=50$) and has density $\rho_a=100$ kg/m^3 ($p=0.077$). The aerogel exhibits a network of uniform fibers (diameter 30–60 Å) with surface area 905 m^2/g. The scattering intensity monotonically decreases

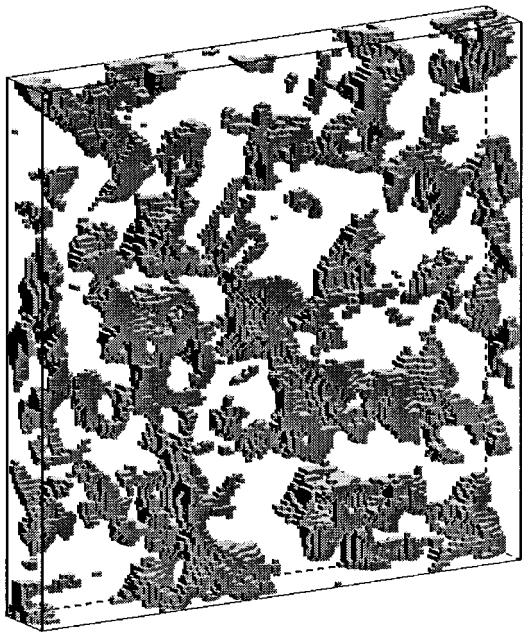

FIG. 2. A model *colloidal* aerogel (solid fraction $p=11\%$). The parameters are $r_c=10$, $\xi=14$, $d=46$ nm, and $p_{\alpha,\beta}=0.07,0.40$. The image is $276\times276\times34.5$ nm. The slab is part of a periodic cubic sample of side length 276 nm (128 pixels). Many of the apparently isolated clusters are interconnected outside the volume shown.

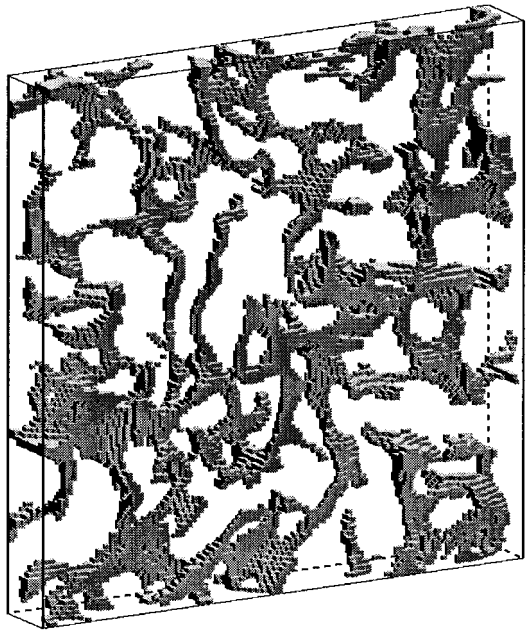

FIG. 3. A model *polymeric* aerogel (solid fraction $p=7.7\%$). The model parameters are $r_c=10$, $\xi=20$, $d=30$ nm, and $p_{\alpha,\beta}=0.36,0.64$. The image is $90\times90\times11.25$ nm.

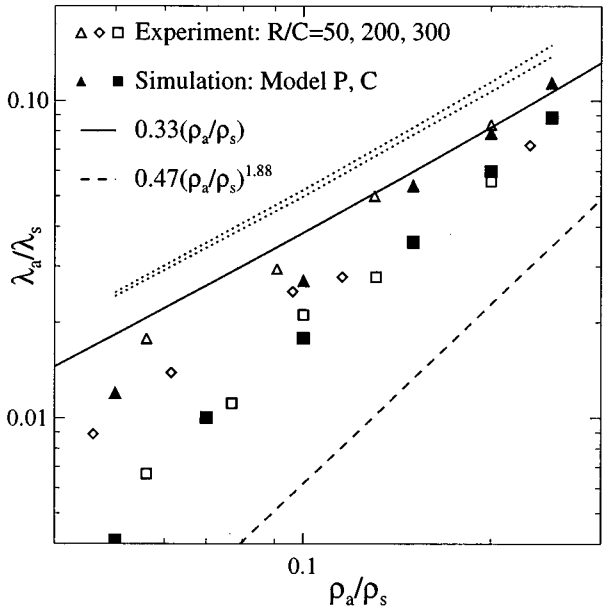

FIG. 4. Solid thermal conductivity of RF aerogels; theory vs experiment [6] ($\rho_s=1300$ kg/m^3, $\lambda_s=0.18$ W m^{-1} K^{-1}). The estimates of λ_a from this work (solid symbols) show very good agreement with experimental data (open symbols). The solid and dashed lines correspond to predictions of λ_a discussed in the text. The dotted lines are rigorous upper bounds.

with q and yields a Guinier radius of 81 Å [8]. In this case we take $r_c=10,\xi=20$, and $d=30$ nm and centered level cut parameters ($\alpha=-\beta$) $p_{\alpha,\beta}=0.361,0.639$. The model has a surface area of 927 m^2/g and a Guinier radius of 101 Å. Figure 1 shows good agreement between the model and experimental scattering curves. A slab of the model material is shown in Fig. 3. The fibers have a relatively uniform thickness, varying from 20 to 60 Å.

As the presence of a peak in the scattering may yield information about the the physical processes underlying aerogel formation [8,12], it is interesting to comment on its morphological origins. The existence of a domain (or repeat) scale in a random structure leads to decaying oscillations in the correlation function, and hence a peak in $I(q)$. In aerogels the decay scale is controlled by the width of the fibers w_f, and the domain scale d is that of the pores. If d is only several times larger than w_f (e.g., the colloidal model) a peak is observed. On the other hand, if d is an order of magnitude larger than w_f (as it is in the polymeric model) the oscillations in $p_2(r)$ are smoothed by a stronger decay and the peak is extinguished (Fig. 1). Note that pores with a well defined scale are evident in the model (Fig. 3); they simply do not carry sufficient statistical weight to appear in the scattering.

We now compare the thermal conductivity of the model to experimental data. The *solid* thermal conductivity of RF gels has been experimentally measured over the density range $\rho_a=60-400$ kg m^{-3} at catalyst concentrations ($R/C=50$, 200, and 300) [3,6]. To estimate the model conductivity we assume that the local heat flux obeys the Fourier law $\boldsymbol{j}=-\lambda(\boldsymbol{r})\nabla T$, where $\lambda(\boldsymbol{r})=\lambda_s(0)$ in the solid (void) phase. Conventional numerical techniques are used to solve the heat conservation equation $\nabla\cdot(\lambda\nabla T)=0$ in a 128^3 lattice subject to an applied temperature gradient [20]. The aerogel conductivity is obtained as $\lambda_a=\langle\lambda(\boldsymbol{r})\nabla T\rangle/\langle\nabla T\rangle$.

Note that we have derived models of colloidal and polymeric aerogels based on the morphology and scattering data at a specific density. We can extend the model to higher and lower densities by making simple assumptions about the density dependence of the model parameters. A simple scaling argument shows the pore scale varies as $d\propto p^{-1/2}$[4] and for simplicity a similar dependence is assumed for r_c and ξ (the conductivity is relatively insensitive to length scale variations [20,30]). The polymeric morphology of the high catalyst ($R/C=50$) aerogels was reproduced by ''centering'' the level cut parameters ($\alpha=-\beta$) (Fig. 3). We preserve this feature of the model by choosing $p_\beta=\frac{1}{2}+\frac{1}{2}\sqrt{p}$ and $p_\alpha=\frac{1}{2}-\frac{1}{2}\sqrt{p}$. The thermal conductivity of the polymeric model ''P'' is shown in Fig. 4. While slightly underestimating the conductivity of the aerogel produced at $R/C=50$, it is nevertheless seen to be in very good agreement with the experimental data. At low catalyst concentration ($R/C=300$) the aerogel morphology was modeled by noncentered level cuts ($\alpha\neq-\beta$) (Fig. 2). To maintain an asymmetry we choose $p_\beta=0.3+\frac{1}{2}\sqrt{p}$ and $p_\alpha=0.3-\frac{1}{2}\sqrt{p}$. The thermal conductivity of this model ''C'' is presented in Fig. 4, providing excellent agreement with the experimental data for the RF aerogel produced at $R/C=300$.

In Fig. 4 we have also plotted a number of results arising from theoretical considerations. Zeng *et al.* [36] have suggested that periodic open-cell models can be used to estimate aerogel conductivity. At low relative densities the ''square rod'' model leads to the estimate $\lambda_a/\lambda_s=\frac{1}{3}\rho_a/\rho_s$ [30] in remarkably good agreement with the data for polymeric RF aerogels. From considerations of phonon heat transport in solids it has been suggested that $\lambda_a/\lambda_s=\rho_a v_a/\rho_s v_s$, where $v_a(v_s)$ is the sound velocity in the aerogel (solid) [37]. Measurements performed on RF aerogels have determined that $v_a/v_s=0.47(\rho/\rho_s)^{0.88}$ so that $\lambda_a/\lambda_s=0.47(\rho_a/\rho_s)^{1.88}$

[4,38]. The result is seen to significantly underestimate the measured conductivity of RF aerogels. It is also possible to calculate rigorous variational bounds [39,40] on the model thermal conductivity [20,30,35]. The upper bounds, which can have predictive power [19,30], are seen to considerably overestimate the true conductivity. Thus theoretical microstructure-property relations are unable to predict the thermal conductivity, and numerical simulations must be relied on.

The agreement between the model and experimental data for both colloidal and polymeric aerogels provides strong evidence that we have accurately modeled the morphology of organic aerogels. The results also indicate that Fourier's continuum theory of heat conduction may hold even in nanoscale structures (diameter 30–60 Å). Of course there is no guarantee that the model is correct: other models may share the same morphological [22] and thermal properties. Nevertheless the utility of the model has been shown. It should be possible to apply the model in the study of gas and radiative conductivity and the mechanical properties of aerogels. The fractal properties of silica aerogels can also be incorporated [35].

Extensions of the model are relevant to a wider range of heterogeneous materials. For example, the solid phase of the aerogel model mimics the intergranular pores of sandstone, and microporosity can be simulated by including random structures at smaller scales. Spheres [19] may be embedded in the models, and closed cell morphologies, such as those observed in solid foams [31], can be formed from the *union* set of two two-level cut GRFs. The model correlation functions can be calculated, allowing surface areas, scattering curves, and rigorous property bounds to be evaluated [35].

[1] *Aerogels*, edited by J. Fricke (Springer, Heidelberg, 1986).
[2] J. Fricke, J. Non-Cryst. Solids **146&147,** 356 (1992).
[3] X. Lu *et al.*, Science **255,** 971 (1992).
[4] L. W. Hrubesh and R. W. Pekala, J. Mater. Res. **9,** 731 (1994).
[5] J. Fricke *et al.*, J. Heat Transfer **117**, 1055 (1995).
[6] X. Lu *et al.*, J. Non-Cryst. Solids **188,** 226 (1995).
[7] D. W. Schaefer and K. D. Keefer, Phys. Rev. Lett. **53,** 1383 (1984).
[8] R. W. Pekala and D. W. Schaefer, Macromol. **26,** 5487 (1993).
[9] D. W. Schaefer *et al.*, J. Non-Cryst. Solids **172-174,** 647 (1994).
[10] A. Hasmy *et al.*, Phys. Rev. B **50,** 6006 (1994).
[11] R. W. Pekala, J. Mater. Res. **24,** 3221 (1989).
[12] D. W. Schaefer, R. Pekala, and G. Beaucage, J. Non-Cryst. Solids **186,** 159 (1995).
[13] R. W. Pekala, C. T. Alviso, and J. D. LeMay, J. Non-Cryst. Solids **125,** 67 (1990).
[14] G. A. M. Reynolds *et al.*, Phys. Rev. B **50,** 18950 (1994).
[15] G. W. Scherer, C. Alviso, R. Pekala, and J. Gross (unpublished).
[16] P. Meakin, Phys. Rev. Lett. **51,** 1119 (1983).
[17] M. Kolb, R. Botet, and R. Jullien, Phys. Rev. Lett. **51,** 1123 (1983).
[18] E. A. Chandler and D. F. Calef, J. Non-Cryst. Solids **186,** 356 (1995).
[19] S. Torquato, Appl. Mech. Rev. **44**, 37 (1991).
[20] A. P. Roberts and M. Teubner, Phys. Rev. E **51,** 4141 (1995).
[21] J. W. Cahn, J. Chem. Phys. **42,** 93 (1965).
[22] S. Marčelja, J. Phys. Chem. **94,** 7259 (1990).
[23] M. Teubner, Europhys. Lett. **14,** 403 (1991).
[24] H. D. Politzer and M. B. Wise, Astrophys. J. **285,** L1 (1984).
[25] J. A. Quiblier, J. Colloid Interface Sci. **98,** 84 (1984).
[26] M. B. Isichenko, Rev. Mod. Phys. **64,** 961 (1992).
[27] N. F. Berk, Phys. Rev. Lett. **58,** 2718 (1987).
[28] A. P. Roberts and M. A. Knackstedt, J. Mat. Sci. Lett. **14,** 1357 (1995).
[29] M. A. Knackstedt and A. P. Roberts, Macromolecules **29,** 1369 (1996).
[30] A. P. Roberts and M. A. Knackstedt, Phys. Rev. E **54,** 2313 (1996).
[31] L. Gibson and M. Ashby, *Cellular Solids: Structure and Properties* (Pergamon Press, Oxford, 1988).
[32] M. Teubner and R. Strey, J. Chem. Phys. **87,** 3195 (1987).
[33] P. Debye, H. R. Anderson, and H. Brumberger, J. Appl. Phys. **28,** 679 (1957).
[34] A. Emmerling and J. Fricke, J. Non-Cryst. Solids **145,** 113 (1992).
[35] A. P. Roberts (unpublished).
[36] S. Q. Zeng, A. J. Hunt, and R. Greif, J. Heat Transfer **117**, 1055 (1995).
[37] O. Nilsson *et al.*, High Temp.-High Pressures **21,** 267 (1989).
[38] J. Gross and J. Fricke, J. Non-Cryst. Solids **145,** 217 (1992).
[39] M. Beran, Nuovo Cimento **38,** 771 (1965).
[40] G. W. Milton, Phys. Rev. Lett. **46,** 542 (1981).